2018 Annual American Control Conference (ACC)
June 27–29, 2018. Wisconsin Center, Milwaukee, USA

Countering Sensor Drift in X-ray Microscopy with Fast and Robust Optimal Control*

Sheikh T. Mashrafi, Curt Preissner, and Srinivasa M. Salapaka

Abstract— **In X-ray microscopy it is imperative that the relative position between the optics stage, that carries the X-ray focusing optics, and the sample stage follow a certain trajectory while either the optics or sample stage is being scanned. Main challenges in achieving this requirement include - open loop drift, environmental disturbance, measurement noise, sensor drift, and control hardware limit. The state-of-the-art in X-ray microscopy at Advanced Photon Source (APS) at Argonne National Laboratory (ANL) features an H_∞ control architecture applied to only the optics stage or both the optics and sample stage, achieving the objectives of large tracking bandwidth over 200 Hz, good positioning resolution on the order of nanometers, rejection of environmental disturbance, attenuation of measurement noise, good X-ray diffraction image resolution and increased imaging bandwidth. However, an unaddressed issue in our existing robust control design is that the sensors and the fixtures that hold the sensors drift with time due to changing air temperature in the APS beamline. Since the drift of sensor itself is not measured, it affects the relative position between the focusing optics and sample resulting into imaging artifacts and reduced image resolution. In this article, we demonstrate the rejection of the sensor drift by directly measuring the displacement of the sensor with respect to the global reference frame. Both the measured sensor displacement (i.e. sensor drift) and optics stage displacement are incorporated in the H_∞ control architecture to achieve the above mentioned objectives in addition to minimal relative displacement between the optics stage and the sample stage. This will improve the X-ray image resolution and reduce image artifacts.**

I. Introduction

APS, the brightest light source in the western hemisphere, provides high-energy, high-brightness and highly penetrating X-rays for scientists and researchers from around the globe to conduct wide range of X-ray science studies such as structure and function determination of materials, observing molecular interactions to develop better pharmaceutical drugs, understanding behavior of minerals in Earth's lower mantle and core, and improving nanoscale electronics. The APS Upgrade (APS-U) project that started on 2011 will provide 100 times brighter coherent X-rays compared to the current APS. Brighter beams of X-rays, with a higher coherent fraction, will result in more compact focused spot, which gives the capability of collecting more detailed data in shorter time. The higher energy X-ray beams have more penetrating capability. The bright and high energy X-rays would enable X-ray imaging of fast events such as biological processes in living organisms in real-time with more details. To complement APS-U fast and robust scanning of the X-ray microscope optics stage in real-time with nanometer to sub-nanometer positioning resolution and large operating bandwidth is necessary.

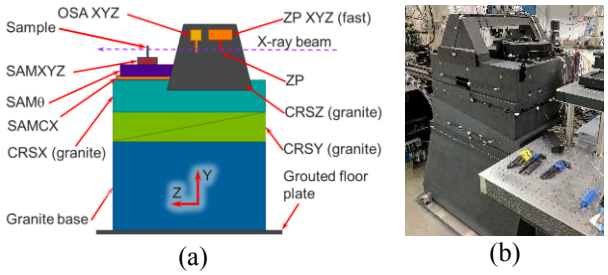

Figure 1. (a) Schematic diagram of the Velociprobe X-ray microscope, (b) the installed instrument at APS beamline.

Velociprobe (Fig. 1), a next-generation X-ray microscope, is built to complement the APS-U. It consists of a novel in-house coarse positioning stage and a state-of-the-art commercially available scanning nanopositioning stages. The coarse positioning stages are made of granite, which provides coarse motion utilizing state-of-the-art air bearing on granite. During X-ray imaging the coarse positioning stages remain static and the air bearing that is supporting the granite blocks are turned off. This makes all the coarse positioning stages and the top gantry act as one granite block, resulting in to good isolation from the environmental disturbance.

Fig. 2 shows the nanopositioning optics stages of the Velociprobe X-ray microscope on a table setup before being assembled on to the Velociprobe granite stages (shown in Fig. 1) at the APS beamline. The Physik Instrumente (PI) 3DOF XYZ nanopositioning optics stage is bolted to an Aluminum alloy reference frame. All the interferometric sensor heads, that are being used for optics and sample stage displacement measurement, are attached to this reference frame. The fixtures that hold the sensor heads at fixed predesignated location are also made with Aluminum alloys.

*Research supported by APS, ANL.

S. T. Mashrafi is with the Mechanical Science and Engineering Department, University of Illinois at Urbana-Champaign, Urbana, IL 61801 USA (corresponding author phone: 217-721-9361; e-mail: mashrafi.sheikh@gmail.com).

C. Preissner is with the X-ray Science Division at the Advanced Photon Source, Argonne National Laboratory, Argonne, IL 60439 USA (e-mail: preissner@aps.anl.gov).

S. M. Salapaka is with the Mechanical Science and Engineering Department, University of Illinois at Urbana-Champaign, Urbana, IL 61801 USA (e-mail: salapaka@illinois.edu).

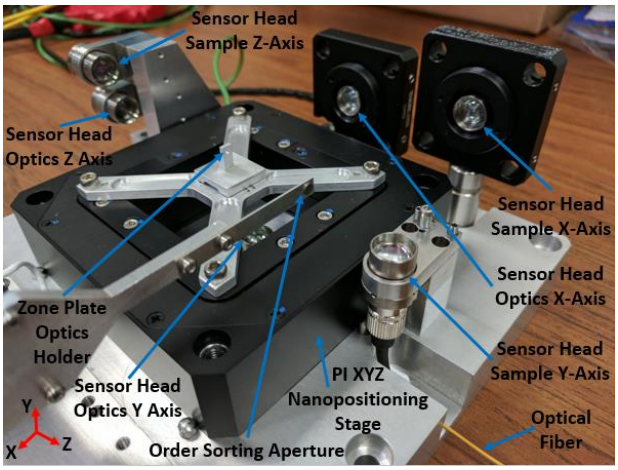

Figure 2. Velociprobe fine scanning optics stage and laser interferometer sensors for stage displacement measurement is shown during assembly on a table. The PI XYZ nanopositioning stages were chosen as the optics scanner. The zone plate optics holder is attached kinematically on the cross-shaped Aluminum alloy fixture, which is in turn bolted on to the PI stage. For displacement measurement of the optics stage, mirrors are glued on the zone plate holder, so that the laser coming out of the standard Attocube focusing sensor heads can reflect back to the sensor heads. The sensor heads for the purpose of the displacement measurement of the sample stage is also attached to the reference frame.

The goal of the Velociprobe X-ray microscope is to scan one-micron square area on the sample in less than 10 seconds and achieve X-ray diffraction images with around 10 nanometers spatial resolution. Here, scanning encompasses the time to move focused X-ray spot on the sample following along a predefined trajectory all the while recording the intensity of the diffracted X-rays hitting the area detector. Previously, that is, before Velociprobe existed, the X-ray microscopes at APS would require more than 1.2 hours to scan the same one-micron square area.

We have developed the state-of-the-art positioning system at APS with the Velociprobe X-ray microscope. We have implemented an H_∞ optimal control architecture that has achieved around 200 Hz -3 dB tracking bandwidth for all three optics nanopositioning stage axes [1]. 3σ-positioning resolution of 1.5 to 3.0 nanometer was achieved for the optics nanopositioning stages [1]. X-ray imaging time, with the H_∞ controllers running on the Velociprobe nanopositioning stages, for the same one-micron area was reduced 8 folds, while guaranteeing spatial image resolution around 13 nanometers. With previous X-ray microscopes the imaging time for one-micron square area would be around 2 hours with worse spatial image resolution.

However, this control architecture does not address the effects of the thermal drift of the sensors that measure the stage displacement. In this article, we are presenting a technique that measures the sensor drift (for both optics and sample stages) in real time and incorporates it into the optimal control problem to minimize the effect of the sensor drift on the optics stages scanning and eventually on the X-ray image. Also we explain fundamental limitations on achievable bandwidth that is imposed by the non-minimum phase zeros of our optics stage. The analysis is well corroborated by experimental results reported earlier articles.

II. X-RAY IMAGING & CHALLENGES

A. Description of X-ray Microscopy at APS

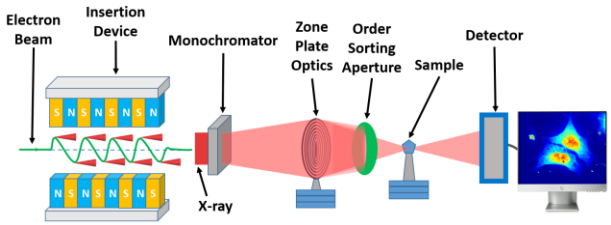

Figure 3. Schematic diagram of Scanning Transmission X-ray Microscopy (STXM) technique for X-ray imaging at a synchroton light source such as APS.

Schematic diagram of the Scanning Transmission X-ray Microscopy (STXM) is a conventional X-ray imaging technique at the APS, shown in the schematic of Fig. 3. The APS electron storage ring, with a circumference of over one kilometer, maintains an electron beam at an energy level of 7 GeV. X-rays are produced from the electron storage ring utilizing the insertion devices placed at a certain interval around the ring. The insertion devices are made of a series of electro-magnets, which alters the path of the electrons or vibrates them as they pass through. This agitation results in photons to be emitted that makes up a wide-band X-ray beam. This wide-band X-ray beam is passed through a monochromator to selectively choose X-rays around a particular frequency with minimal spread. The X-ray beam is then focused as a spot on to the sample with the zone-plate focusing optics. This focused X-ray spot is then scanned along a predefined trajectory to cover a target region of the sample. The high-energy highly-penetrating X-rays or photons interacts with the sample molecules and as a result gets diffracted in different directions. These diffracted X-rays are detected by an area detector downstream of the sample as intensity data. Based on this recorded diffraction intensity information and algorithmically recovered phase information the 2D or 3D image of the scanned region of the sample is reconstructed. The X-ray images from the STXM technique gives an impression of the internal structure and function of the sample with 10-20 nanometer spatial resolution.

B. Current State-of-the-art for Feedback Control

The articles [1], [2], and [3] showcases the H_∞ control architecture implemented on X-ray microscope scanning stages at the APS. The Early User Instrument (EUI) [1] was the first X-ray microscope optics scanning stages on which the H_∞ optimal control algorithm was implemented and resulted into significant improvement in open loop drift or actuator drift rejection, tracking bandwidth (up to 33 Hz and 86 Hz -3 dB bandwidth for X and Y stage respectively) and 3σ positioning resolution (up to 3.3 nanometer and 1.9 nanometer for X and Y stages respectively). Further improvement has been done with the Velociprobe nanopositioning stages [1], [2]. -3 dB bandwidth of 200 Hz have been achieved for all of the X, Y, and Z optics stages [1], giving an improvement of 606% and 232% for X and Y stages compared to EUI, respectively. The implemented H_∞ controllers for the Velociprobe optics fine-scanning stages are targeted to be high bandwidth controllers, because that is suitable for the step scan technique of X-ray

imaging. These high bandwidth controllers are not designed for high resolution application. The 3σ positioning resolution for Velociprobe optics stages are 3.0, 2.9, and 1.5 nanometers for X, Y, and Z stages, respectively [1].

C. Impact of the Sensor Drift on X-ray Microscopy

To reconstruct high spatial resolution X-ray image of a sample the zone-plate focusing optics needs to be scanned with high-precision stages in closed-loop with controllers featuring large positioning bandwidth and high positioning resolution. These controllers acting on the optics stage in real-time directly reduces the open loop drift of the scanning stages, rejects any incoming environmental disturbances and attenuates measurement noise of the sensor. Above architecture works out perfectly when the assumption that the sensor is fixed with respect to the global reference frame. The fiber interferometric position sensor being used for measuring the scanning stage displacements are mounted on aluminum alloy fixtures on the reference frame. As a result, the interferometric sensor heads slowly drift with time due to the thermal expansion and contraction of the aluminum alloy fixtures due to air temperature fluctuations observed at the APS beamline. Since the drift of the sensor itself is not measured, it is erroneously registered as optics stage movement resulting in faulty correction of the stage position. Due to this faulty motion of the optics stage the incoming X-rays are focused as spot off-target on the sample resulting into imaging artifacts.

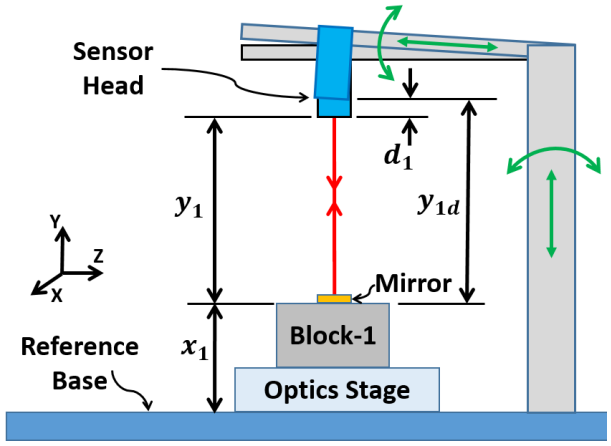

Figure 4. Schematic diagram showing the effect of thermal drift of the sensor and the sensor fixture.

Fig. 4 shows the schematic of the optics stage displacement measurement by laser interferometric sensor. Where, x_1 is the actual stage displacement with respect to the global reference frame, and y_1 is the measured displacement of the optics stage. Due to thermal drift of the Aluminum alloy sensor fixtures the sensor head itself drifts by a distance of d_1. This movement can be erroneously registered as the stage displacement by the sensor, giving the new measured displacement to be y_{1d}. The corrective action of the feedback controller would actually move the optics stage by the amount of d_1 to wrong coordinates in space, which in turn will focus the X-ray in a different spot on the sample, away from the reference trajectory. This will introduce X-ray imaging artifacts, image stitching errors and reduce the achievable spatial image resolution. The alignment tolerance for the Attocube interferometric focusing sensor head that is used for this experiment is ± 2 degrees for a working distance up to 10 mm and smaller tolerance for larger working distances. So, the small angular rotation resulting from the thermal drift of the sensor fixtures will not take the sensor off alignment during X-ray imaging.

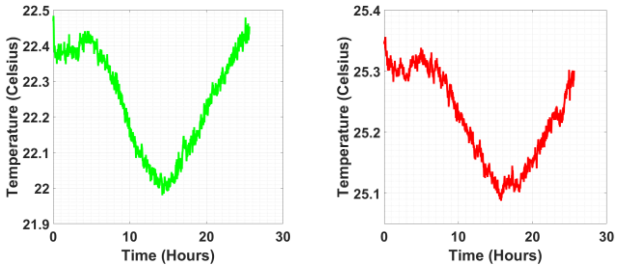

Figure 5. Over 24 hour temperature log recorded at the APS beamline. (a) the air temperature in the experimental hutch, and (b) the sample stage temperature measured at the base.

Fig. 5 shows the air temperature and the sample stage temperature measured for over 24 hours at APS beamline where the Velociprobe is installed. The maximum variation of the air and sample stage temperature over 24 hours is 0.5 and 0.25 degree Celsius, respectively. Since, the sample stage and sample stage fixtures are mostly made with Aluminum alloy, this would mean a 100 mm long Aluminum alloy section would thermally drift by 600 nanometers in the 24-hour time frame. Similar effect would be observed for the optics stage sensor fixtures as well. As mentioned at the beginning, the relative motion between the optics stage and the sample stage should follow a predefined trajectory with nanometer to sub-nanometer level positioning resolution for the highest quality X-ray image. Thermal drift occurring in the sensor fixtures can very easily affect the X-ray image quality by introducing image ambiguity, image stitching error, and other imaging artifacts.

D. Current State-of-the-art for Sensor Drift Rejection

All the work that has been done with the X-ray microscopes positioning stages at the APS [1], [2], and [3] addresses objectives of actuator drift minimization, robust stability, large tracking bandwidth, good positioning resolution, good disturbance rejection and adequate noise attenuation in real-time. There is no existing mechanism of countering the effect of drift of the sensors themselves with respect to the global reference frame. The existing literature, regarding the other synchrotron sources, covers some methods (linear, non-linear drift model) to counter actuator drift in the post-processing part of X-ray imaging, but does not refer to the sensor drift.

E. Limitations of Current State-of-the-art Feedback Control

One of the major hurdles for controller design is the presence of right half plane (RHP) zeros in the X, Y, and Z optics stage models. Since, controllers are designed based on these experimentally identified stage models, these zeros are present in the closed-loop sensitivity transfer function S. These zeros influence the shape of the S transfer function and makes it hard to achieve large tracking bandwidth. For Velociprobe optics stages the open loop bandwidth is over 1 kHz. But due

to presence of RHP zeros the achievable closed-loop bandwidth was just over 200 Hz [1]. This limitation was observed for the previous EUI X-ray microscope optics scanning stages as well [3].

F. Requirements of Different Scanning Technique

The two main scanning technique used in X-ray imaging are the step scan and the fly-scan. In step scan technique, to do a raster scan to cover a one-micron square area on the sample, the optics stage is first given a command to move to position 1 on the first row of the raster. Then it is verified through measurement that the stage has indeed moved to the desired position 1, resulting in some time delay. At this point, the diffraction data starts getting recorded by the photon detector for a predefined time ensuring the correct dose of photons. After the data is recorded the detector requires a short gap during which it cannot record any more data. After this, the command to move to position 2 (one step right in the same row of the raster) is given. So, clearly the step scan requires significantly longer time due to different overheads involved. In addition, the step movement involves high frequency components like a square wave. This introduces a closed-loop tracking bandwidth requirement that can only be met by controllers with large -3 dB tracking bandwidth [1]. The controllers designed to give high 3σ positioning resolution have low -3 dB tracking bandwidth, and hence are not suitable for step scan technique. The X-ray images achieved in [1] are with large -3 dB tracking bandwidth controllers running on the optics scanning stages during a typical step scan routine. Fly-scan technique in short, requires the optics stages to be moved continuously all the while collecting the X-ray diffraction data at a predefined interval. Due to continuous motion requirement during fly-scan, reference trajectories can have a single frequency component, such as circular or Lissajous trajectories and so on. This means high resolution controllers that have smaller -3 dB tracking bandwidth will be adequate for a fly-scan that will cover the same one-micron square area in much less time compared to the step scan.

III. Optimal Control Approach

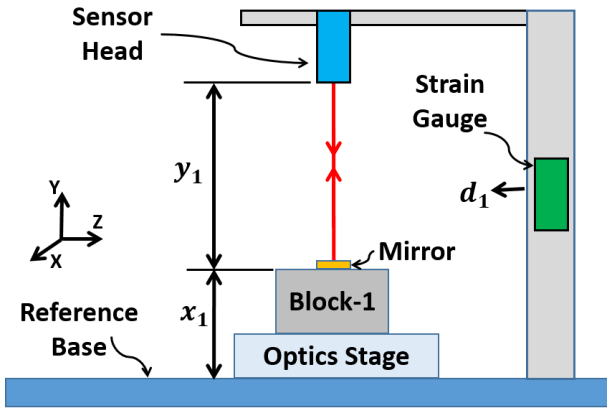

Figure 6. Schematic diagram showing the measurement of sensor drift, d_1 using a strain gauge sensor attached to a key location on the sensor fixture.

To counter the sensor drift d_1 (Fig. 6), we are measuring the drift in real time with an additional sensor and incorporating this measurement in the optimal control algorithm. The control algorithm would ensure precise positioning of the optics stage with respect to the global reference frame while remaining unaffected by the drifting sensor. The other closed-loop objectives of large tracking bandwidth, good positioning resolution, environmental disturbance rejection, measurement noise attenuation will also be achieved by the optimal control algorithm. A strain gauge sensor is chosen to measure the drift in the Aluminum alloy fixtures on which the laser interferometer sensor heads are attached. The sample stage displacement y_2 and sample stage drift d_2 (measured with a separate strain gauge sensor) would also be incorporated in the optimal control algorithm to ensure minimum relative displacement between the optics and sample stage. A strain gauge sensor capable of measuring strain $\Delta L/L$ in the range of 6-12 microstrains with a resolution of 0.01 microstrains would be sufficient for measuring the sensor fixture drift. The bandwidth requirements on the strain gauge sensor is not very high since thermal drift is a slow process with the time-scale being on the order of hours. Multiple strain gauge sensors can be employed at different location of the fixture, as needed, and the algebraic sum of the strain measurements can be used to calculate the total drift.

A. Feedback Control Architecture

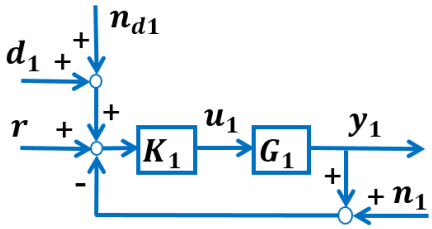

Figure 7. Transfer function block diagram of the negative feedback control architecture for the sensor drift rejection scheme. Here, G_1 is experimentally identified optics stage model (along one axis), K_1 is the designed controller, y_1 is the optics stage displacement, d_1 is the optics stage drift, n_1 and n_{d1} are the measurement noise for the stage position and sensor drift.

The transfer function block diagram in Fig. 7 shows sensor drift d_1 being introduced in the feedback loop. Our goal from the fine-scanning of optics stages point is to achieve good tracking and minimize the tracking error, $e = r - y_1 - d_1$. Here

$$y_1 = T_1(r - d_1 - n_1 - n_{d1}). \quad (1)$$

$$e = S_1(r - d_1) + T_1(n_1 + n_{d1}). \quad (2)$$

Where, $S_1 = 1/(1 + G_1K_1)$ is the sensitivity transfer function and $T_1 = G_1K_1/(1 + G_1K_1)$ is the complementary sensitivity transfer function. To achieve good tracking, we would like to have $T_1 \approx 1$ in the frequencies of the reference signal r and also T_1 needs to be small in the high frequencies where measurement noise n_1 and n_{d1} are predominant. This would make (1) approximately equivalent to $y_1 \approx r - d_1$, where $r - d_1$ can be thought of as the reference the stage should track to eliminate the effect of drift. To minimize the tracking error e, we need to make S_1 small in the frequencies of the reference signal r and in the low frequencies which is characteristic of thermal drift d_1, effectively making the term $S_1(r - d_1)$ small. Also, T_1 needs to be small in the high frequencies to minimize the second term $T_1(n_1 + n_{d1})$ in tracking error.

B. H_∞ Optimal Control Architecture

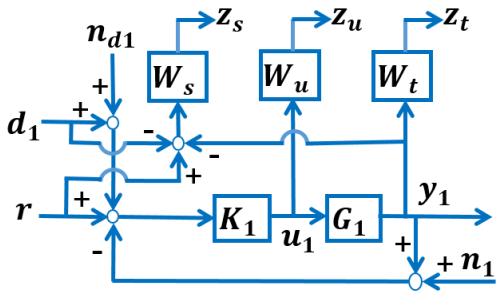

Figure 8. Transfer function block diagram of the H_∞ minimization problem, which incorporates the measured sensor drift d_1 in the optimal control architecture. Here, W_s, W_t, and W_u are the design weights and z_s, z_t, and z_u are the regulated outputs.

The transfer function block diagram for the H_∞ mixed-sensitivity minimization problem is shown in Fig. 8. The closed-loop objectives are achieved simultaneously by choosing appropriate design weight W_s, W_t, and W_u. The weighted tracking error $z_s = W_s(r - y_1 - d_1)$, weighted stage displacement $z_t = W_t y_1$, and weighted control output $z_u = W_u u_1$ are the regulated output signals corresponding to the tracking bandwidth, noise attenuation and control effort closed-loop objectives. The closed-loop transfer function matrix T_{wz} from exogenous inputs $w = [r - d_1 \quad n_1 \quad n_{d1}]$ to regulated outputs $z = [z_s \quad z_t \quad z_u]$ is minimized to achieve the closed-loop objectives. The optimal control algorithm K_1 is obtained by solving the minimization problem $\inf_{K_1} \|T_{wz}\|_\infty$.

The design weights shape the closed-loop transfer functions S_1, T_1, and K_1S_1. The sensitivity weight W_s is designed to have a have a low-pass filter shape, so that S_1 gets high pass filter shape, which effectively makes the tracking error small in the reference trajectory frequencies. The complementary sensitivity weight W_t is chosen to have a high pass filter shape, which makes T_1 to have a low pass filter shape; $T_1 \approx 1$ in low frequencies for good tracking and small in high frequencies for measurement noise attenuation. To bound the controller output the control effort weight W_u is chosen so that it keeps K_1S_1 small in bandwidth frequencies.

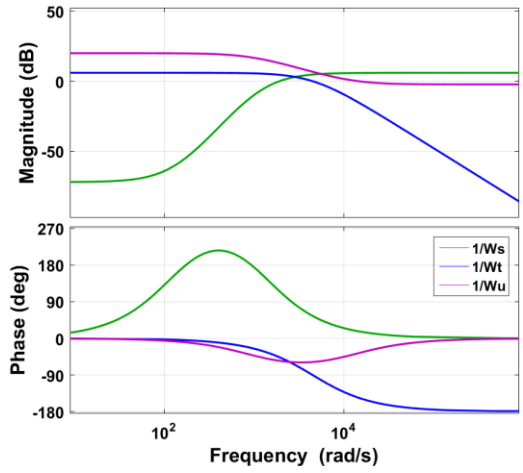

Figure 9. Bode diagram of the design weights W_s, W_t, and W_u for a particular H_∞ controller design.

The design weights for a H_∞ controller K_1 is shown in Fig. 9. The inverse of the sensitivity design weight $1/W_s$ has a large -3 dB bandwidth so as to achieve a similar high-pass filter shape for the sensitivity transfer function S_1. The inverse of the complementary sensitivity weight $1/W_t$ has a low-pass filter shape so as to make T_1 approximately equal to one in low frequencies and small in high frequencies.

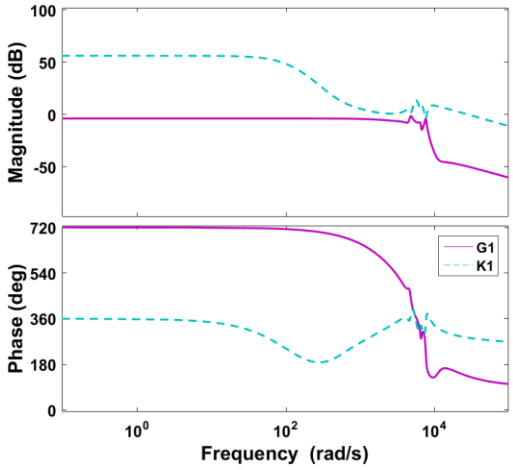

Figure 10. Bode diagram of the Velociprobe vertical Y-stage model G_1 and the designed H_∞ controller K_1.

Fig. 10 shows the Bode diagram of the Velociprobe nanopositioning vertical Y-stage model G_1 and the H_∞ controller K_1 designed based on this stage model. Significant reduction of sensor drift, large tracking bandwidth, robust stability, environmental disturbance rejection, measurement noise attenuation to some extent was achieved by the controller K_1.

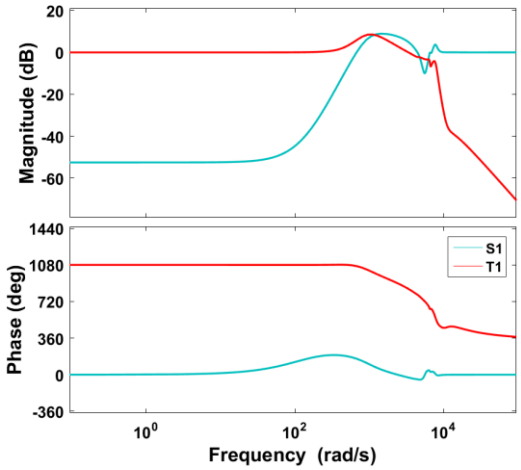

Figure 11. Bode diagram of the closed-loop transfer functions S_1 and T_1.

The designed closed-loop sensitivity transfer function S_1 and complementary sensitivity transfer function T_1 is shown in the Fig. 11. Clearly, $T_1 \approx 1$ in low frequencies giving good tracking characteristics and small in high frequencies where measurement noise is predominant. S_1 is small in low frequencies and rises over -3 dB level at a much higher frequency resulting in small tracking error, minimizing the effect of sensor drift d_1 and rejecting any environmental disturbance.

IV. RESULTS

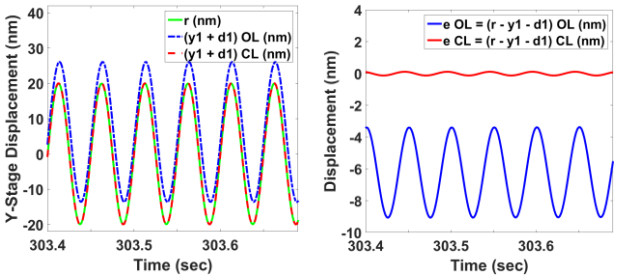

(a) (b)

Figure 12. (a) Comparison of open loop and closed-loop tracking for a sinusoidal reference trajectory with 20 nanometer amplitude and 20 Hz frequency. (b) Tracking error $e = r - y_1 - d_1$ comparison between open loop and closed-loop.

The reference tracking comparison between open loop and closed-loop for the 1DOF H_∞ controller K_1 is shown in Fig. 12a. The open loop stage position is slowly drifting away due to the artificially introduced thermal drift d_1 (approximately 600 nanometers per 12-15 hour) in simulation. Compared to that the closed-loop position is tracking the reference trajectory quite closely, due to the small sensitivity transfer function S_1 value in the frequencies of the thermal drift and the reference signal. Fig. 12b shows the comparison of tracking error e between the open loop and the closed-loop. The closed-loop tracking error is less than 1% of the reference signal and as expected is significantly less than the open loop.

The achievable closed-loop bandwidth with the H_∞ controller is limited due to the presence of RHP zeros in the experimentally identified optics stage model. These RHP zeros made the peak of the sensitivity transfer function S_1 rise way beyond the 6 dB introducing lack of robust stability for the controller designs with larger tracking bandwidth. The complementary sensitivity transfer function T_1 peaked close to the -3 dB S_1 bandwidth frequency for these large tracking bandwidth controllers. This peak in T_1 means the lack of good tracking (in terms of amplitude) close to the bandwidth frequencies. This is not acceptable for step scan X-ray imaging technique, since the stage displacement (1) might get wrongly scaled by T_1. Similar, peaking phenomena on both S_1 and T_1 were observed while designing for high resolution controllers. This is fundamental limitation can be explained by the second Bode integral law

$$\int_0^\infty \ln|S(j\omega)| \frac{2z}{z^2+\omega^2} d\omega = 0, \qquad (3)$$

which imposes a finite waterbed effect, since from the integrand above we can show that there exists $\omega < \infty$ such that $\int_\omega^\infty \ln|s(j\omega)| \frac{2z}{z^2+\omega^2} d\omega < \epsilon$ for any $\epsilon > 0$. This implies that low values of $|S(j\omega)|$ at low frequencies will result in high peaks in $|S(j\omega)|$; thereby compromising on robustness to modeling uncertainties. From these fundamental limitation integral constraint, we show that for robustness quantified by $S_{max} \approx 6\,dB$, tracking error at low frequencies specified by $|S(j\omega)| < -40\,dB$, and assuming a 40 dB/decade rise of $|S(j\omega)|$, the maximum possible tracking bandwidth is approximately 200 Hz, which matches with our simulations and experiments.

V. CONCLUSION

The sensor drift measurement in real time to reduce the effect of sensor drift in X-ray image shows promising results in simulation. The strain gauge sensors to measure thermal drift of the laser interferometer sensor fixture should work out in experiment similar to the simulations. The sensor drift rejection will lead to more precise positioning of the optics stage and eventually scanning the focused X-ray spot along a more precise trajectory on the sample. This would be beneficial for long X-ray imaging experiments, which is more prone to sensor drift as well as actuator drift. Due to presence of RHP zeros and the limiting upper bound on the achievable tracking bandwidth it introduces, it would be beneficial to invest resources on the optics scanning stage codesign with the controller architecture in mind. Optics scanning stages with higher stiffness and RHP zeros pushed towards higher frequency region and beyond the resonant frequency would significantly increase the achievable tracking bandwidth in closed-loop. Fly-scan technique would enable the use of controllers with lower -3 dB S_1 bandwidth and the T_1 transfer function that starts falling off at lower frequencies resulting in better positioning resolution.

ACKNOWLEDGMENT

S. T. Mashrafi thanks Christian Roehrig, Junjing Deng, Paul Rossi, Michael Fries and rest of the Velociprobe team for their support.

Argonne National Laboratory's work was supported by the U.S. Department of Energy, Office of Science, Office of Basic Energy Sciences, under contract DE-AC02-06CH11357.

REFERENCES

[1] S. T. Mashrafi, C. Preissner, S. M. Salapaka, "The Velociprobe: pushing the limits with fast and robust control," in *32nd ASPE Annual Meeting, 2017*.

[2] S. T. Mashrafi, C. Preissner, S. M. Salapaka, "Fast scanning of X-ray optics an optimal control approach," in *31st ASPE Annual Meeting*, 2016.

[3] M. Borland, "Ultra-low-emittance light sources," in *Synchrotron Radiation News, 27(6), 2-2, 2014.*

[4] J. Maser, B. Lai, T. Buonassisi, Z. Cai, S. Chen, L. Finney, S. C. Gleber, C. Jacobsen, C. Preissner, C. Roehrig, V. Rose, D. Shu, D. Vine, S. Vogt, "A next-generation hard X-ray Nanoprobe beamline for in situ studies of energy materials and devices," in *Metallurgical and Materials Transaction A, volume 45, issue 1, pp 85-97, 2014.*

[5] S. T. Mashrafi, C. Preissner, S. M. Salapaka, H. Zhao, "Something for (almost) nothing: X-ray microscope performance enhancement through control architecture change," in *28th ASPE Annual Meeting, 2013*.

[6] R. P. Winarski, M. P. Holt, V. Rose, P. Fuesz, D. Carbaugh, C. Benson, D. Shu, D. Kline, G. B. Stephenson, I. McNulty, and J. Maser, "A Hard X-ray Nanoprobe Beamline for Nanoscale Microscopy," in *Journal of Synchrotron Radiation, volume 19, pp 1056-1060, 2012.*

[7] C. Lee, S. M. Salapaka, "Robust broadband nanopositioining: fundamental trade-offs, analysis, and design in a two-degree-of-freedom control framework," in *Nanotechnology, volume 20, number 3, 2009.*

[8] A. Sebastian, S. M. Salapaka, "Design methodologies for robust nanopositioning," in *IEEE Transactions on Control Systems Technology, volume 13, number 6, 2005.*